Optical properties of ordered and randomly disordered AlAs/GaAs short-period superlattices

D. J. Arent, R. G. Alonso, G. S. Horner, D. Levi, M. Bode, A. Mascarenhas, and J. M. Olson
National Renewable Energy Laboratory, 1617 Cole Boulevard, Golden, Colorado 80401

X. Yin and M. C. DeLong
Department of Physics, University of Utah, Salt Lake City, Utah 84112

A. J. SpringThorpe and A. Majeed
Bell Northern Research, Limited, P.O. Box 3511, Station C, Ottawa, Ontario, Canada K1Y 4H7

D. J. Mowbray and M. S. Skolnick
Department of Physics, University of Sheffield, Sheffield S3 7RH, United Kingdom
(Received 19 July 1993; revised manuscript received 27 December 1993)

The optical properties of different atomic arrangements of $Al_{0.5}Ga_{0.5}As$, deposited by molecular-beam epitaxy and having nominally identical average composition, have been compared. Markedly different signatures are seen in steady-state, time-resolved, and microwave-modulated photoluminescence, photoreflectance, and photoluminescence-excitation spectroscopies for a random pseudobinary alloy and $(AlAs)_n(GaAs)_{4-n}$ superlattices where $n=2$ (ordered) or n is randomly chosen (disordered) from the sets [1,2,3] or [0,1,2,3,4]. When n=[0, 1, 2, 3, or 4] the optical properties are dominated by quantum confinement effects due to the presence of layers with thicknesses up to 14 monolayers. When n=[1, 2, or 3] the optical properties are consistently described by the presence of disorder-induced localized states and a hopping-assisted recombination mechanism.

I. INTRODUCTION

In the past, increased degrees of freedom for device design and successful use of semiconductor material properties, such as band-gap energy and the lattice constant, have been achieved primarily by altering the composition. Periodic crystalline structures such as superlattices (SL's) allow for an additional degree of freedom in band-structure engineering through proper choice of layer thicknesses and composition. Similar periodic changes in composition also occur spontaneously in ternary alloys,[1] in which alternate isoatomic planes contain nonrandom distributions of the component atomic species. Spontaneous ordering, though relatively easily induced during epitaxial growth,[2] is inhomogeneous and difficult to reproduce in detail, adversely affecting transport properties.[3] This inhomogeneity introduces ambiguity in the interpretation of experimental findings for these systems, so that it is unclear whether the observed behavior results from the presence of ordering or of the random distribution (disorder) of domains of material with different amounts of order.[1,4,5] Thus we have undertaken a study of homogeneously ordered and disordered materials to elucidate the distinguishable properties.

The observation of carrier localization in one-dimensional random systems was first studied in purposely disordered $GaAs/Al_xGa_{1-x}As$ superlattices, where it was demonstrated that vertical transport in superlattices decreased with increasing disorder.[6] Additionally, it was shown that the vertical transport is thermally activated from localized levels with trap energies of 5–66 meV, depending on the degree of disorder, and that the transport displays behavior characteristic of an Anderson transition as the disorder exceeds a value which leads to the localization of all eigenfunctions [disorder of two monolayers (ML's) was sufficient for complete localization in the SL's studied of nominal width 30 Å].[6,7]

As recently as 1989, severely disordered materials requiring monolayer precision were proposed.[8] These materials, called disordered monolayer superlattices (d-SL's), are composed of randomly distributed layers with thicknesses L_z no greater than 6 Å, and an average disorder of $L_z/2$. A disordered monolayer superlattice, for example, composed of an alternating sequence of 1 ML of GaAs followed by 3 ML of AlAs, then 2 ML GaAs, 2 ML AlAs, 3 ML GaAs, 1 ML AlAs, etc., would produce a random superlattice with an overall periodicity of 4 ML and average composition of $Al_{0.5}Ga_{0.5}As$. This sequencing is in contrast to a normal, ordered superlattice of the same dimension, where 2 ML of GaAs and 2 ML of AlAs are repeatedly deposited in alternating sequence, or a bulk alloy where both Ga and Al atoms impinge on the growing surface at the same time (no intentional spatial separation).

Initial monolayer d-SL studies concentrated on the AlAs/GaAs system, where investigations have shown that d-SL layers exhibit (1) increased photoluminescence (PL) and electroluminescence intensity, especially near 300 K, compared to ordered and bulk alloy equivalent materials; (2) reduced band-gap energies relative to com-

positionally equivalent random alloys and ordered superlattices of the same, or even longer, periodicity; (3) a temperature dependence of PL intensity similar to that of amorphous materials, which is described by $I \propto [1 + A \exp(T/T_0)]^{-1}$, where T is absolute temperature, T_0 is the characteristic temperature corresponding to the energy depth of localized states from a mobility edge, and A is a tunneling factor; and (4) a shorter PL decay lifetime than equivalent indirect-gap alloys or ordered SL's.[8-13] The luminescent behavior was observed to depend on the probability distribution of the layer thicknesses, and was attributed to different localized states created by the disordering in atomic arrangement.[13] Some experiments have also been performed on GaP/AlP,[14] and CdSe/ZnSe (Ref. 15) d-SL's. The results of these experiments and early theoretical treatments[16-18] support the assignment of the observed properties to localization effects similar to those ascribed to amorphous materials and Anderson localization.[19]

In this paper, we have addressed two crucial issues with respect to monolayer d-SL materials: the influence of the (dis)ordering deposition sequence (randomization) on the optical properties of d-SL materials, and the reproducibility of sensitive optical properties of d-SL's when epitaxially deposited in different molecular-beam-epitaxy (MBE) chambers using growth conditions different from those previously reported.[8] We present extensive analysis, using a variety of techniques, of optical properties of the random pseudobinary $Al_{0.5}Ga_{0.5}As$ alloy and related artificially ordered and disordered [001] superlattice structures deposited by MBE.

II. EXPERIMENT

In the present study, we focus on microstructures consisting of stacks of four monolayer units along the [001] direction, where each unit is composed of $(GaAs)_n(AlAs)_{4-n}$. The following samples were grown by solid source MBE on exact [001] GaAs substrates: (i) a three-dimensional (3D) random binary alloy (RBA) of $Al_{0.5}Ga_{0.5}As$; (ii) a $(GaAs)_2(AlAs)_2$ [001] ordered superlattice [to be denoted as o-(2,2) SL]; (iii) a $(GaAs)_n(AlAs)_{4-n}$ [001] disordered superlattice where $n = 1,2$, or 3 is a random number [$d-(1,3)$]; and (iv) a $(GaAs)_n(AlAs)_{4-n}$ [001] disordered superlattice where n is varied randomly from the set [0,1,2,3,4], denoted as $d-(0,4)$, and the $n = 0$ component indicates that the layer is skipped. A significant variation in the sequencing of the GaAs and AlAs layers, relative to those employed in previous studies,[8] was used: we have maintained a short-range period of 4 ML. That is, the layer sequences we have employed are defined as $(GaAs)_n(AlAs)_{4-n}$, whereas those previously studied[8] were formulated as $(GaAs)_n(AlAs)_m$ ($n,m = 0$–4 or n, $m = 1,2,3$; n and m are independently randomly determined). In each d-SL we have studied, the probability of occurrence for each n was equal.

Undoped samples were grown by MBE on semi-insulating, 50-mm-diameter GaAs substrates, which were mounted indium-free, under As_2. Growth rates were calculated from calibration growths employing both *in situ* infrared interference measurements and *ex situ* reflectometry.[20,21] Following oxide desorption under As_2 at ~640 °C, a 500-Å GaAs buffer was grown. Each sample included a 0.5-μm-thick $Al_{0.5}Ga_{0.5}As$ reference layer grown at 640 °C. The SL's were grown without the use of growth interrupts at a low growth rate of 0.25 ML/s and a low growth temperature of 560 °C to maximize interface abruptness and limit cation diffusion.[22] These conditions contrast those used in previous studies: 600 °C and 3–5-s growth interrupts with a growth rate of 0.5 ML/s.[8] The d-SL layers were 0.3 μm thick and capped by 100 Å of GaAs. Aluminum concentration, sample thickness, and periodicity were confirmed by double-crystal x-ray diffraction and transmission electron microscopy (TEM).

In order to structurally characterize the SL's and to verify their structure, TEM and transmission electron diffraction (TED) experiments were performed on the structures. All samples were prepared in a cross section by mechanical thinning and final ion milling with Ar^+ at 3.5 kV. All observations were done with the electron beam parallel to a ⟨110⟩ zone axis, also enabling limited high-resolution imaging.

Optical analysis included photoluminescence (PL), photoreflectance (PR), microwave-modulated PL (MMPL),[23] photoluminescence excitation spectroscopy (PLE), and time-resolved PL (TRPL).[24] Conventional PL was performed with continuous 488-nm Ar^+ laser excitation, and detected with either single-photon-counting techniques or using an S-20 photomultiplier (PMT) and conventional lock-in techniques at a chopping frequency of 100 Hz. Both modifications of the PL technique gave similar results. Selectively excited PL and PLE were excited with the focused monochromatic light from a 150-W tungsten lamp or a dye laser using DCM dye, dispersed with a 0.85-m double monochromator and detected with a cooled GaAs PMT. In the latter case, the dc output from the GaAs PMT was recorded directly. The lamp excitation was 1–5-mW/cm^2; the intensity of the focused dye laser was much higher, typically 240 W/cm^2. The excitation intensity varied throughout the PLE scans, and the spectra were corrected for this variation. Data were collected from 5 to 300 K and over a range of excitation intensities from 0.03 mW/cm^2 to 230 W/cm^2. We obtained PR spectra at 5 K using the 6328-Å line of a 1-mW He-Ne laser, chopped at 100 Hz, as the pump beam. The probe beam was generated with a 150-W tungsten lamp and monochromator. Critical-point energies were extracted from PR spectra by least-squares fitting the spectra to the Aspnes third derivative functional form.[25]

Microwave-modulated PL (MMPL) is a spectroscopy in which a sample is placed in the electric field maximum of a $TE_{(011)}$ 16-GHz microwave cavity and subjected simultaneously to continuous optical excitation (typically on the order of 1 W/cm^2 at 488 nm), and pulsed microwaves at a power on the order of 5 mW. Changes in luminescence intensity that result from applying the microwave electric field are detected with standard phase-sensitive techniques at the microwave chopping frequency and phase. Interpretation of the results of these experiments is discussed below.

III. RESULTS

A. Transmission electron microscopy

1. The o-(2,2) SL

Figure 1(a) shows an experimental {110} diffraction pattern of the o-(2,2) SL. The extra spots at $\frac{1}{2}(001)$ positions are clearly visible and sharp, attesting to the high quality of the sample.

2. The d-(1,3) SL

Figure 1(b) shows a diffraction pattern from the d-(1,3) SL. This image was recorded with the electron beam parallel to a [100] zone axis, while the diffraction patterns of Figs. 1(a) and 1(c) were taken with the electron beam parallel to a [110] zone axis. In all cases, extra spots at $\frac{1}{2}(001)$ positions are present. This d-SL sample also exhibits extra spots at the $(2/n)(001)$ positions, with $n=5,6,7,\ldots$. These spots are accompanied by streaking in the (001) direction, which is associated with the random layer thicknesses.

3. The d-(0,4) SL

This random sequence of GaAs and AlAs layers also introduces a periodicity into the crystal which is identical to that of the o-(2,2) SL. In addition, larger periodicities (5,6, etc.) may be present due to the incorporation of the $n=0$ subunit. For example, the GaAs layer thickness could exceed $n=4$ by growing a 4-0-3-1 sequence, which would result in an $n=7$ layer of GaAs. The diffraction pattern will display these additional periodicities as extra spots at $(2/n)(001)$ positions, with $n=5,6,7,\ldots$. Figure 1(c) shows the experimental diffraction pattern of the sample. The spots at the predicted positions are clearly visible. Spots with $n>7$ are spaced too closely to the matrix spots to be distinguished, and thus appear as intensity spikes in the (001) direction. Double diffraction effects lead to further streaking of the individual extra spots.

Figure 2 shows a (004) dark-field image of the same sample. The random sequencing of AlAs and GaAs layers is clearly visible as bands with low and high intensities of varying widths. The relatively wide dark band located in the upper section of the image is formed by growth of a $(GaAs)_2(AlAs)_2$ subunit followed by two $(GaAs)_4(AlAs)_0$ sequences, which effectively leads to a $(GaAs)_{10}$ layer. The interfaces between GaAs and AlAs appear very abrupt and smooth. A quantitative analysis of the interfacial quality, however, requires the application of advanced high-resolution methods, like chemical mapping, which will be presented in another publication.

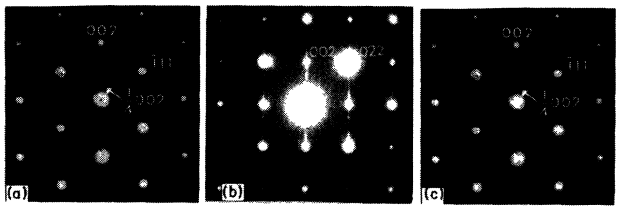

FIG. 1. Transmission electron diffraction image of (a) o-(2,2) SL, (b) d-(1,3) SL, and (c) d-(0,4) SL. The extra spots near the $\frac{1}{2}(001)$ positions confirm the long-range order of the SL samples. The additional spotty streaks in (b) and (c) are associated with the random sequencing employed, which effectively produces sections of the SL with longer periodicity. Note that Figs. (a) and (c) were taken with the electron beam parallel to a [110] zone axis, while Fig. (b) was recorded with the electron beam parallel to a [100] zone axis.

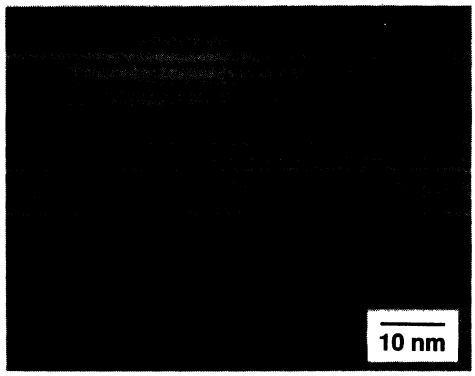

FIG. 2. A (004) dark-field transmission electron micrograph of the d-(0,4) SL displaying periodic variations associated with the random sequencing of the GaAs and AlAs layers. The relatively wide dark band located in the upper portion of the image is produced with the sequence $(AlAs)_2(GaAs)_2$ followed by two $(GaAs)_4(AlAs)_0$ subunits, effectively producing a $(GaAs)_{10}$ layer.

B. PL and PLE

PL and PLE spectra from the four samples are plotted in Figs. 3–5. By varying the deposition sequence of the group-III atoms (Ga and Al) in structures having identical average composition, we have been able to change the peak emission energy by more than 0.2 eV, as well as numerous other spectral details.

The PL and PLE spectra obtained from the RBA and o-(2,2) SL (Fig. 3) show relatively weak PL emission associated with the lowest-energy indirect transition $E_{X-\Gamma}$ at $\sim$2.05 eV and phonon replicas similar to earlier findings.[26] For the RBA sample, the PL is a broad manifold upon which sharp peaks are superimposed, with a full width at half maximum (FWHM) as small as 5.1 meV. The PLE spectrum [detected at 2.066 eV; arrow in Fig. 3(a)] shows a well-resolved free excitonic absorption at 2.148 eV, giving a Stokes shift of 82 meV. Separate PLE spectra were obtained with the detection energy set to each of the four peak energies. All PLE spectra showed free excitonic absorption. The maximum emission intensity is at 2.037 eV; the peak separations [see labels, Fig. 1(a)] are consistent with the LO-phonon energies of GaAs (X) (31 meV) and AlAs (X,Γ) (48 meV).[26] These PL and PLE spectra are in agreement with those previously published, and serve as a benchmark against which to contrast other spectra.

In comparison, the optical signature of the o-(2,2) SL [Fig. 3(b)] is dominated by a single emission at 2.052 eV, 15 meV lower than the high-energy PL emission from the

RBA, and phonon replicas. PLE detected at the PL peak energy indicates a weak excitonic absorption with a band-gap energy of 2.150 eV. Reduction of the PL emission energy relative to the RBA without a significant change in the absorption characteristics is consistent with the predicted type-II pseudoindirect nature of the lowest-energy transition[27] and earlier observations.[26] The PL intensity from the RBA and *o*-(2,2) samples decays rapidly and rather uniformly (i.e., independent of energy) with increasing temperature to ~40 K (not shown), in agreement with earlier findings.[12,26] Additionally, the PL peak shape is relatively independent of excitation intensity.

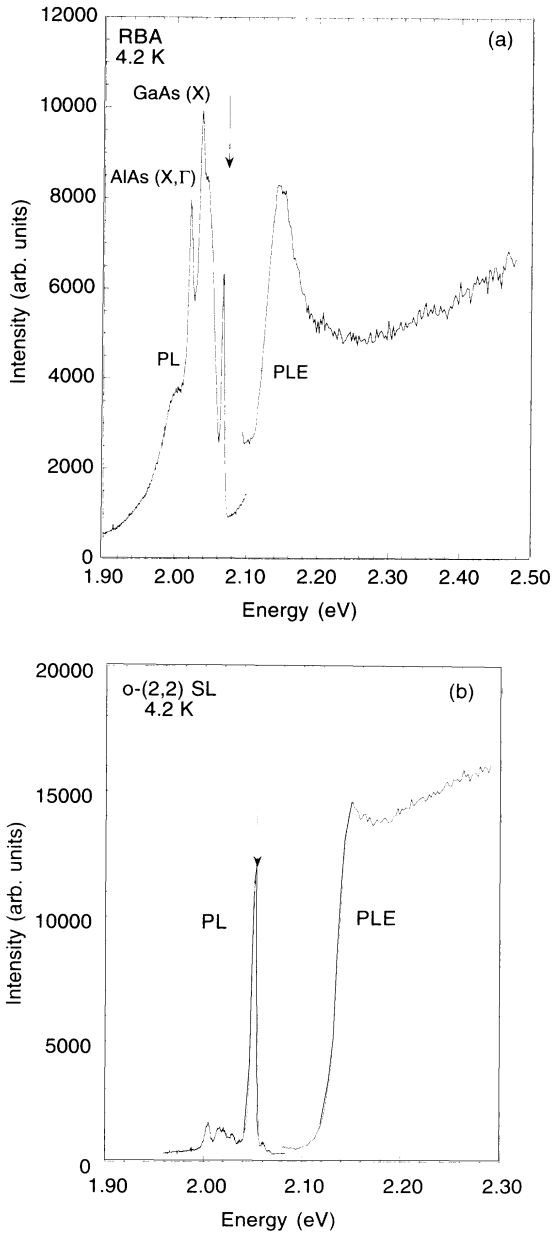

FIG. 3. Photoluminescence and photoluminescence excitation emission as a function of photon energy taken at 4.2 K for (a) $Al_{0.5}Ga_{0.5}As$ RBA, and (b) $(GaAs)_2(AlAs)_2$ ordered SL. Excitation intensity was 5 mW/cm^2 at 5400 Å. The arrows indicate the detection energies used to collect the PLE spectra.

As seen in Figs. 4(a) and 5(a), the PL and PLE spectra from the *d*-SL samples are remarkably different from those of the RBA and the *o*-(2,2) SL. The 4-K PL spectrum of the *d*-(1,3) SL excited at 2.3 eV [Fig. 4(a)] exhibits a strong peak at 1.926 eV with up to five shoulders. Also, PL excited at 1.941 eV is nearly half as intense as that excited at higher energy (2.032 eV), indicating that a significant density of states exists at the lower energies. In all cases the peak at 1.926 eV (with FWHM=9.4 meV) dominates the spectrum. Introducing the *d*-(1,3) randomization sequencing has redshifted the dominant emission by more than 120 meV, similar to previous observations for *d*-SL's formulated as $(GaAs)_n(AlAs)_m$.[8]

As shown in Fig. 4(a), the PLE spectra for the *d*-(1,3) SL display absolutely no indication of the presence of free excitonic absorption. PLE was performed with the detection energy set at each of the discernible peaks. Representative spectra from the two most intense peaks (1.926 and 1.936 eV) and the highest-energy shoulder (1.964 eV) are shown in Fig. 4(a) and labeled curves (*ii*), (*iii*), and (*iv*), respectively. In contrast to the sharp absorption edges seen in the PLE spectra of the RBA and *o*-(2,2) SL, these PLE spectra show broad absorption tails extending down to at least 2.03 eV. Detecting at the peak energy of 1.926 eV, trace (*ii*), the absorption edge is redshifted to 1.986 eV, 186 meV from the pseudobinary alloy absorption edge energy. Under intense 200-W/cm^2 excitation, further decreasing the PLE detection energy moves the absorption edge even farther to the red, with the lowest detectable absorption edge at 1.925 eV, 225 mV below the band-edge energy of the pseudobinary alloy. We ascribe the observed optical properties to the presence of tail states extending to low energy, well below the highest emission energy. Such a description is consistent with strong localization, where the required nonperiodic potential has been synthetically produced by using a random deposition sequence for the group-III atoms.[6,28] Also indicative of the existence of a large density of states at lower energy is the fact that emission from the three lowest-energy bands could be excited at an energy of 2.032 eV (not shown). All PLE spectra show a very ill-defined band edge and absorption tails to very low energy, particularly compared to the sharp edges of the RBA and *o*-(2,2) samples.

We observed additional evidence for the complex nature of the *d*-(1,3) SL sample in the changes in peak energy and spectral line shape of PL with temperature and excitation intensity [Figs. 4(b) and 4(c), respectively]. For PL obtained with unfocused 514-nm Ar^+ excitation at approximately 1.2 W/cm^2, the emission from the higher-energy 1.926-eV transition decreases in intensity much more rapidly than that from the lower-energy transition at 1.905 eV as the sample temperature increases. Since the band-gap energies of the component materials GaAs and AlAs and the RBA change only slightly over the temperature range of interest, and since both emissions are observed at 5 K, the observed changes in spectral line shape are most probably due to a strong competition among recombination pathways rather than simple tem-

perature dependence of the band gap. These observations are consistent with carrier trapping in shallow potential wells[6,28] where moderate increases in temperature provide the carriers with sufficient excess energy to escape and cascade to lower energy minima. It is worth mentioning that this is true only if the structure is composed of many shallow wells, with only a few deeper PL emission states. If this were not the case, the low-energy transition would remain dominant as $T \rightarrow 0$ K.

Photoluminescence spectra taken over four orders of magnitude in excitation intensity are presented in Fig. 4(c) for the d-(1,3) SL. The low excitation intensity PL spectrum of the d-(1,3) SL shows emission at 1.925 eV. As the incident intensity increases, processes at higher and lower energy dominate. Such behavior may result from energy levels with a low density of states and/or long lifetime becoming saturated. Stronger emission will be observed from states with shorter lifetimes or higher densities. As higher-energy states become populated, new recombination paths become available (for example,

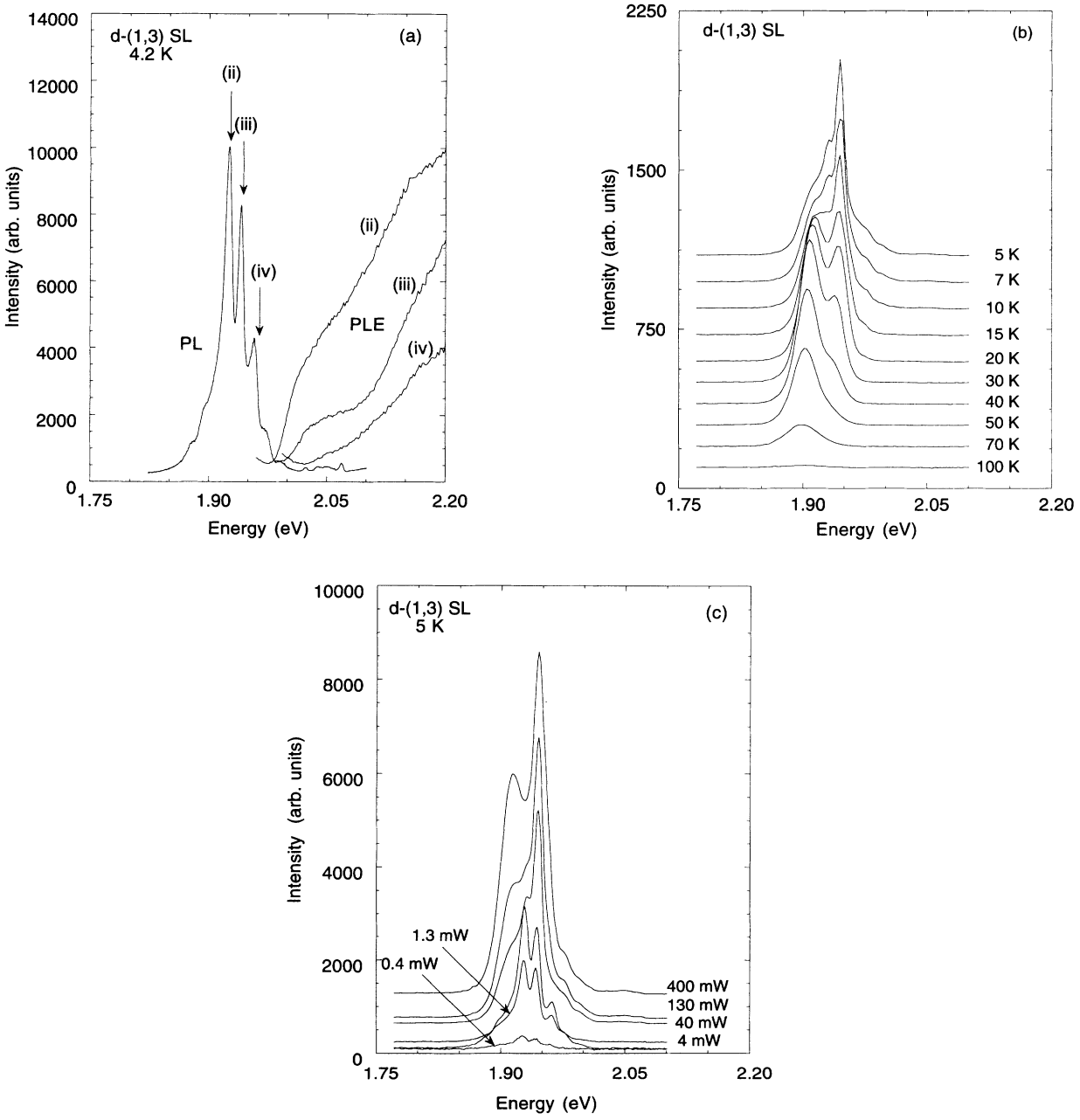

FIG. 4. (a) PL and PLE emission as a function of photon energy for the d-(1,3) SL. The sample temperature was 4.2 K, and the excitation intensity was 5 mW/cm^2 at 540 nm. The arrows indicate the detection energy used to collect the PLE spectra with increasing energy from curves (*ii*)–(*iv*). (b) PL emission plotted for different sample temperatures using 40-mW unfocused 488-nm Ar^+ excitation, offset vertically for clarity. (c) PL emission plotted for different excitation intensities of an unfocused 488-nm Ar^+ laser. The sample temperature was 5 K, and spectra are enlarged and offset for comparison.

electrons may spatially diffuse to nearby lower-energy states) and new emission processes at lower energies may turn on. In marked contrast, the profile of PL spectra of the RBA and *o*-(2,2) (not shown) and *d*-(0,4) SL's [see Fig. 5(c)] change very little with increasing excitation intensity.

The PL spectrum of the *d*-(0,4) SL is qualitatively different from those described previously in that the spectral features are individually resolved, as shown in Fig. 5(a). Seven reasonably well-defined PL peaks are observed between 1.625 and 1.898 eV. The two highest-energy peaks at 1.880 and 1.898 eV are clearly detected with near-gap, deeply penetrating excitation energies greater than 2.2 eV (i.e., larger than the band-gap energy of the $Al_{0.5}Ga_{0.5}As$ RBA layer). Their intensity is comparatively weak for the shallow-penetrating 488-nm Ar^+ excitation used in Figs. 5(b) and 5(c). Additionally, PLE detected on these two highest-energy emissions show essentially the same sharp, well-defined band edge at ~ 2.17 eV [Fig. 5(a), curve (*iv*)], with no evidence of a

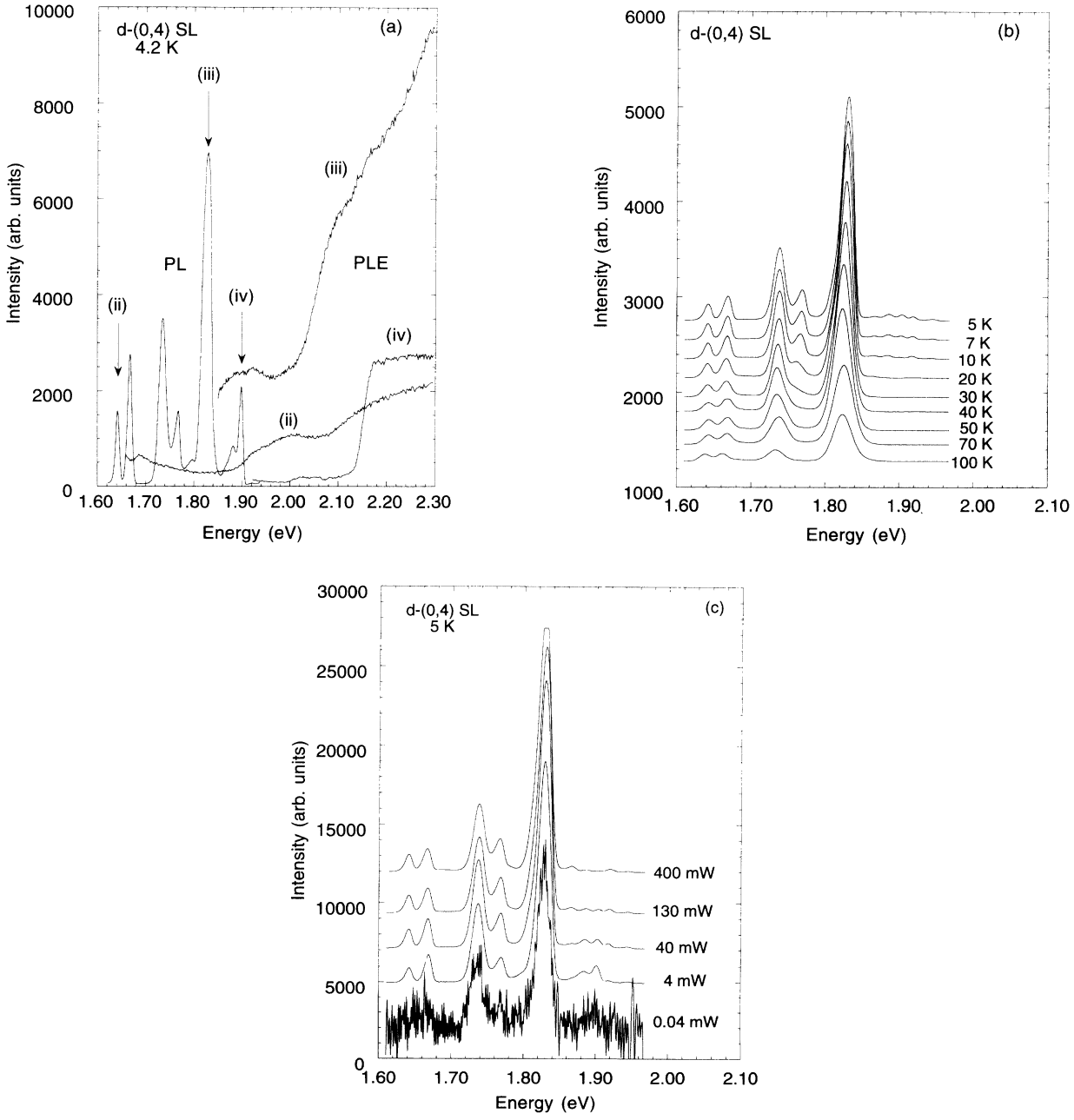

FIG. 5. (a) PL and PLE emission as a function of photon energy for the *d*-(0,4) SL. The sample temperature was 4.2 K, and the excitation intensity was 5 mW/cm^2 at 540 nm. The arrows indicate the detection energy used to collect the PLE spectra with increasing energy from curves (*ii*)–(*iv*). (b) PL emission plotted for different sample temperatures using 40-mW unfocused 488-nm Ar^+ excitation. Spectra are offset, but the scale is constant. (c) PL emission plotted for different excitation intensities of an unfocused 488-nm Ar^+ laser. The sample temperature was 5 K, and spectra are enlarged and offset for comparison.

free excitonic absorption. These properties are consistent with emission processes from regions of the *d*-(0,4) SL that are physically close to the RBA buffer layer and separated from the "bulk" of the *d*-SL by a thin, minimally absorbing AlAs layer.

The PLE spectra detected on the five lower-energy peaks of the *d*-(0,4) SL, [representative spectra are shown in Figs. 5(a), curves (*i*) and (*iii*)] exhibited extremely broad absorption tails without a well-defined band edge. The PLE spectrum detected at 1.826 eV from the highest intensity PL emission shows [Fig. 5(a), curve (*iii*)] an onset at ~1.85 eV as well as one at ~2.05 eV. For the next two lower-energy PL peaks at 1.767 and 1.735 eV, emission can be detected for excitation down to about 1.82 eV. The PL emission at 1.642 eV can be excited down to about 1.66 eV Fig. 5(a), curve (*ii*)]. Note that for the two highest-energy PL peaks, the PLE spectra are essentially energy independent above the band gap. The same is not true of the lower-energy emissions; the PLE spectra decay more or less monotonically over all energy ranges surveyed. One interesting general feature of the *d*-SL samples is the fact that the two highest-energy emissions are very deep states of a very high-energy absorption process, and yet all others are associated with a broad spectrum of absorption processes, each with a distinctive Stokes shift, spectral line shape, and band-gap energy.

Temperature- and intensity-dependent PL spectra for the *d*-(0,4) SL are shown in Figs. 5(b) and 5(c), respectively. In contrast to the previous three samples, there is very little spectral dependence on either temperature or excitation intensity. These observations suggest that the radiative recombination transitions may be fundamentally different from those of the *d*-(1,3) SL; they also suggest that increased carrier localization inhibits migration to nonradiative recombination sites. As previously reported[29] and confirmed by our measurements, the PL emission intensity of the RBA and *o*-(2,2) SL decrease much faster with increasing temperature than either *d*-SL. The PL emission intensity of the *d*-(0,4) SL decreases more slowly than that of the *d*-(1,3) SL. In many respects, the spectra of the *d*-(0,4) SL resembles a collection of isolated "mini"-SL's, each with a unique band gap and absorption profile. In the extreme, these would be considered isolated single quantum wells with relatively ill-defined interfaces, as evidenced by FWHM values ≥ 19 meV in the 4.2-K PL spectra. Due to the finite probability of layers having zero thickness, the *d*-(0,4) SL includes GaAs or AlAs regions with thicknesses greater than 4 ML. In fact, inspection of the actual computer-generated layer sequence reveals GaAs and AlAs layers with thicknesses up to 11 and 14 ML, respectively. AlAs layers with thicknesses greater than 30 Å (11 ML) are effective confining barriers[30] that inhibit miniband formation, suggesting that the *d*-(0,4) SL may have regions that are isolated from strong wave-function overlap with next-nearest-neighboring regions.

C. MMPL

As mentioned above, MMPL is a spectroscopy in which a sample is placed in the electric-field maximum of a microwave cavity and subjected simultaneously to continuous optical excitation and pulsed microwaves. Although not definitive on its own, MMPL is useful in helping to identify specific optical processes and in estimating the relative strengths of electron-lattice coupling in different materials.[31] The immediate effect of the microwave electric field is to heat photogenerated free carriers. The luminescence spectrum may then change as a result of the microwave-field-accelerated free carriers simply raising the lattice temperature, by impact ionizing shallow bound carriers, or by redistributing carriers among the various competing radiative and nonradiative recombination channels in accordance with the energy dependencies of those channels.[31] Hence shallow donors may be ionized, leading to a negative MMPL peak at the donor-acceptor pair energy. The liberated electrons may enhance the associated band-acceptor recombination process, leading to a positive MMPL peak at an energy higher by the donor binding energy. The ratio of the areas of these peaks gives a crude estimate of the importance of nonradiative processes: nearly equal areas indicate that nonradiative processes are unimportant; the absence of positive peaks suggests that nonradiative processes compete efficiently for band carriers. A similar analysis applies to the competition between localized and free excitons, whose signatures are negative and positive (at higher energy) MMPL peaks, respectively. An example of the latter situation is included in Fig. 6, where we show the MMPL spectrum of a conventional $GaAs/Al_xGa_{(1-x)}As$ multiple single quantum well (MSQW) with four isolated GaAs quantum wells having nominal widths of 50, 90, 150, and 780 Å. Associated with the PL for each well is a negative peak at lower en-

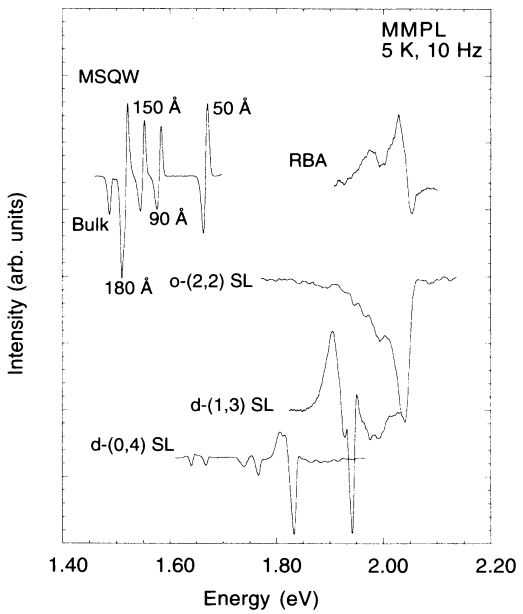

FIG. 6. MMPL as a function of photon energy at 10 Hz for $Al_{0.5}Ga_{0.5}As$ (RBA), *o*-(2,2) SL, *d*-(0,4) SL, *d*-(1,3) SL, and an intentionally grown $GaAs/Al_xGa_{(1-x)}As$ MSQW with four GaAs QW's. Sample temperatures were ~5 K in all cases; the excitation intensity was ~1.2 W/cm^2.

ergy (bound exciton) and a positive peak at higher energy (free exciton). A negative peak is also seen corresponding to the ionization of donors from the donor-acceptor pair process in the bulk (buffer layer). For this system, the interaction between the microwave-heated free carriers and PL is completely nonthermal, i.e., mediated by impact ionization or the energy dependence of the capture cross sections.

Figure 6 also shows representative MMPL spectra of the four $Al_{0.5}Ga_{0.5}As$ samples taken at 5 K at a chopping frequency of 10 Hz, where thermal microwave-PL interactions, if present, are important. In this case, the MMPL spectrum exhibits a strong thermal component. The MMPL signature of the RBA consists of a negative peak at high energy (2.06 eV) and positive peaks at lower energy (2.03 and 1.98 eV). The signs of the thermal components of the MMPL are consistent with the temperature dependence of the PL (not shown) wherein the high-energy peak decays rapidly with increasing temperature while the lower-energy processes decay more slowly or may even increase. The spectrum is consistent with a weakly localized exciton (2.06 eV) being thermally ionized, and some of the resulting electrons and holes contributing to impurity-related processes at lower energy. Two aspects of the MMPL of the RBA are unusual and not at all understood: (1) the strong thermal component of the microwave-PL interaction, which is indicative of strong electron-lattice coupling and usually seen only in conventional naturally ordered materials;[23] and (2) the fact that the thermal and nonthermal components of the MMPL have very different spectral dependences. The latter observation suggests that the nonthermal component of the microwave-PL interaction is mediated by the energy dependence of capture cross sections rather than impact ionization. Such behavior, although rare, has been observed previously in weakly ordered $Ga_{0.5}In_{0.5}P$.[31] The net positive integral also argues for the importance of the energy dependence of the capture cross section as the mediating mechanism.

The MMPL spectrum of the *o*-(2,2) SL sample shows only strong negative signals, indicating that the primary effect of the microwaves is to channel free carriers to nonradiative processes. The interaction is again thermal, characteristic of a strong electron-lattice coupling. In contrast, the near-zero integral from the *d*-(1,3) SL implies that the majority of photoexcited carriers are in disorder-induced localized states and unable to channel to nonradiative processes. However, the fact that the positive signals are at lower energy than the negative ones also indicates that the processes do not have the simple relations seen in high-quality quantum wells (localized and free excitons) or homogeneous bulk materials (donor- and band-acceptor recombination). Specifically, the presence of a negative peak at high energy and a positive peak at lower energy indicates that carriers tend to be ionized from the high-energy emission process and are preferentially captured into the low-energy processes, which is similar to the temperature- and intensity-dependent PL behavior described earlier.

For the *d*-(0,4) SL, the earlier discussion of PL suggested that the structure more closely resembled a series of discrete regions than a single SL with continuous minibanding and a large presence of low-energy states. Significant qualitative differences between MMPL spectra of the *d*-(0,4) SL and real MSQW suggest, at the very least, the presence of a high density of nonradiative centers.

The MMPL results indicate that the optical processes occurring in all of these samples (with the partial exception of the RBA) are *not* the conventionally related ones seen in homogeneous bulk materials or quantum wells; rather they more closely resemble three-dimensionally inhomogeneous, multidomain "ordered" materials.[31]

D. Photoreflectance spectroscopy

We obtained PR spectra at 5 and 300 K (not shown) to investigate the critical points in the joint density of states. We have employed PR, as well as PLE, to probe upward (absorption) electron transitions that are sensitive to the density of states of the band structure. This contrasts with emission measurements, such as PL, that probe downward (recombination) electron transitions where the Boltzmann factor tends to favor lower-energy states. Complementary measurements are necessary to obtain an accurate description of the dominant optical processes. Representative PR spectra taken at 5 K are shown in Fig. 7. As is common among all PR spectra, transitions from the GaAs cap or buffer layer are observed at 1.516 eV from the direct band gap, and 1.85 eV from the spin-orbit-split band. Although each of the signatures in the PR spectra for the *d*-SL samples is reproducible, we have extracted transition energies only for the well-separated transitions because of the complexity and potential ambiguity of the fitting procedure when it is applied to a large number of peaks.

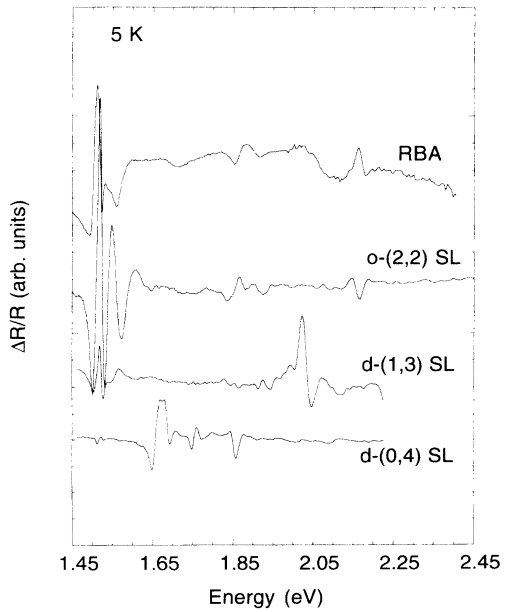

FIG. 7. Photoreflectance as a function of photon energy at 5 K for the $Al_{0.5}Ga_{0.5}As$ RBA, $(GaAs)_2(AlAs)_2$ ordered SL, *d*-(0,4) SL, and *d*-(1,3) SL. Each feature in the spectra of the *d*-SL samples is reproducible.

The PR spectra of the RBA and *o*-(2,2) SL reveal the alloy band-gap energy at 2.166 eV, in excellent agreement with the PLE-determined band-gap energy. We observe the crystal-field-split transitions at 2.031 and 2.054 eV (300 K, not shown) [2.166 eV (5 K), unresolved] for the *o*-(2,2) SL. At 5 K, PR of the *d*-(0,4) sample shows a minimum of five lower-energy transitions over the range 1.6–1.9 eV, whereas the PR spectra from the *d*-(1,3) SL is featureless over this range of energy. These observations, combined with data obtained from PL, suggest, on the one hand, that the lower-energy transitions in the *d*-(0,4) SL are from regions of the *d*-SL matrix that are separated by relatively wide AlAs barriers formed by multiple occurrences of the $(AlAs)_4(GaAs)_0$ subunit and are strongly localized. On the other hand, the *d*-(1,3) SL does not exhibit a broad spectrum of low-energy transitions in either PR or PL, suggesting that the lower-energy PL peak and PR signature (relative to the RBA) may be associated with a large density of band-tail states below the fundamental gap, as suggested by the PL and PLE observations described above. At 300 K (data not shown), both *d*-SL structures show a high-energy signature at ~2.005 eV; its magnitude and line shape suggest that it is associated with the buried $Al_{0.5}Ga_{0.5}As$ layer. At energies below 2.0 eV, reproducible features are observed from 1.55 to 1.9 eV and from 1.8 to 2.0 eV for the *d*-(0,4) SL and *d*-(1,3) SL, respectively. These features, although weak, suggest a relatively substantial density of states at energies well below the fundamental gap of the pseudobinary alloy, again consistent with PLE results.

E. Time-resolved photoluminescence

Time-resolved PL spectra from the *d*-(0,4) SL were taken as a function of temperature from 15 to 300 K, and are displayed in Fig. 8. The decay profiles exhibit multiexponential behavior with time constants in the range of 1–100 ns. These data are summarized in Fig. 9 for 77 K as a function of the energy of the emission peak, and

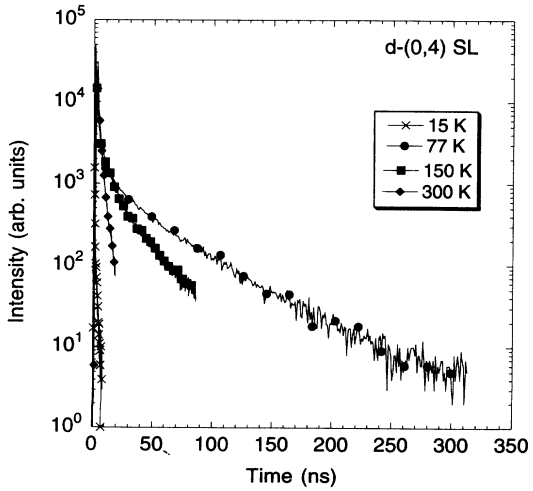

FIG. 8. TRPL intensity detected at 1.82 eV as a function of time for the *d*-(0,4) SL at various temperatures. The profiles observed exhibit pure single or double exponential decays. The symbols are for labeling purposes only. See text for details.

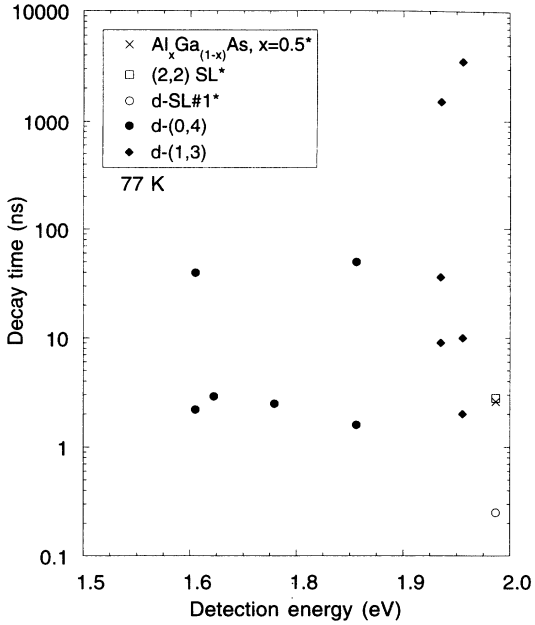

FIG. 9. PL lifetime as a function of emission energy for *d*-(0,4) and *d*-(1,3) SL samples at 77 K. Some data (*) from Ref. 29 have also been included for comparison.

compared to other *d*-SL data in the literature.[11] The long lifetime component measured from the *d*-(0,4) SL decreases with increasing temperature, which is indicative of effective carrier trapping of spatially separated carriers in the strongly disordered structure. These carriers must thermalize from their localized state to the extended states in order to diffuse and meet a recombination partner. The short lifetime component remains at ~0.8 to 2 ns from 15 to 300 K, consistent with the behavior of localized photogenerated electrons and holes with large spatial overlap in the random low-dimensional matrix.[15] We analyzed the temperature dependence of the PL longer lifetime component with a simplified quantum-well (QW) model[32] describing the thermal escape of carriers from localized wells, and we estimate scattering times for the photogenerated carriers of 14–30 ps and effective barrier heights of 10 meV. These results, consistent with our estimate from PL temperature dependence and the above calculations, give an order of magnitude estimate of the effective localization barrier for carriers in the *d*-(0,4) SL.

At 50 K, TRPL profiles from the *d*-(1,3) SL differ markedly from any of the spectra obtained from the *d*-(0,4) SL. As shown in Fig. 10, we observe highly nonexponential decays, displaying a continuously changing slope of PL intensity vs time. The continually increasing PL lifetimes observed in these structures may be explained in terms of carrier localization. The short lifetimes (0.8–2.0 ns) measured at early times are consistent with recombination of electrons and holes localized within the same potential minimum. As time passes, these localized carrier populations are depleted and the bimolecular, intrawell recombination rates become slower due to the necessity of carrier transport. At relatively

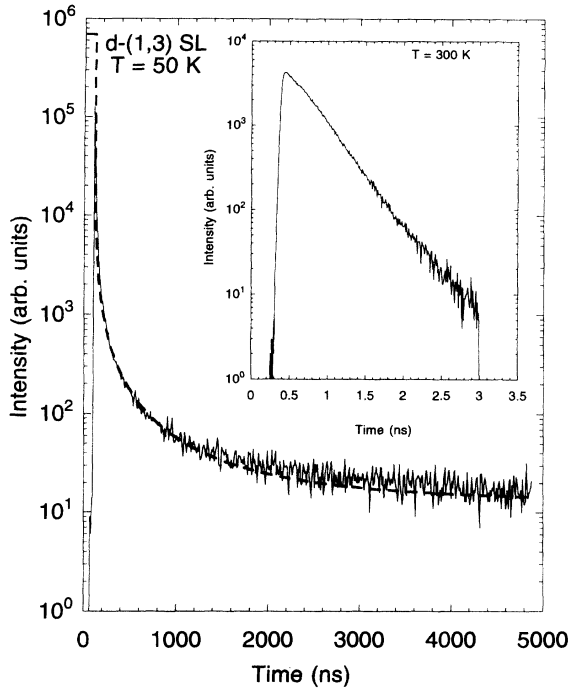

FIG. 10. TRPL intensity detected at 1.919 eV as a function of time for the d-(1,3) SL sample at 50 K. The observed profile can be fitted (dashed line) by a stretched exponential of the form $I=I_0\exp[-(t/\tau)^{\beta}]$, with $\tau=1.4$ ps and $\beta=0.2$. At 300 K, the disorder-induced localization barriers are easily overcome by the thermal energy of the carriers, and hence the decay profile is single exponential, depicted in the inset, with a characteristic lifetime of 350 ps.

long times, carriers are unlikely to find a recombination partner in the same local minimum. Under these conditions, recombination becomes spatially indirect, and vertical (parallel to the growth direction) transport must take place for recombination to occur. Vertical transport can take place via tunneling or hopping conduction. Interestingly, it has been pointed out that, at low temperatures, the most frequent hopping process would *not* be to a nearest-neighbor site.[28] Thus it is likely that carriers in the d-(1,3) SL diffuse across more than one localized minimum, effectively increasing the PL lifetime and enhancing the long-time PL intensity.

The decays fit the functional form $I=I_0\exp[-(t/\tau)^{\beta}]$ that describes long-tailed relaxation of free carriers, where I_0 is the initial intensity, t is time, τ is the characteristic lifetime of free carriers, and β is a scaling factor related to the fractal dimension of the disorder and can be correlated to the ratio T/T_0, where T is the absolute temperature and T_0 is related to the width of the distribution of barriers.[15,32,33,34] This "stretched exponential" description has previously been established to describe hopping-assisted recombination present in many disordered physical systems including porous and amorphous Si and CdSe/ZnSe d-SL's.[15,32,35] The best-fit values of β for the d-(1,3) SL are ~ 0.2, indicating that the distribution of barriers is relatively small (as expected from the growth design) and that at higher temperatures where the carriers have more energy, the barriers should appear more uniform and hence the time distribution narrower.[32] For the d-(1,3) SL, the 300-K TRPL decay profile should be a single exponential. This prediction is unambiguously observable in the inset of Fig. 10, with a best-fit lifetime of 350 ps.

For comparison to other data in the literature,[11] we have extracted best-fit multiexponential decay times for the d-(1,3) SL at 77 K, with three estimable components at ~ 3 ns, 30 ns, and 1 μs, as summarized in Fig. 9. The short-time component of our d-(1,3) SL is an order of magnitude longer than that previously reported for samples without the intentional long-range order, and comparable to lifetimes reported for the indirect type-II $(GaAs)_2(AlAs)_2$ SL at 77 K.[11] We note for comparison that ~ 20-μs lifetimes and nonexponential decay kinetics are observed at 1.8 K for AlAs/GaAs type-II SL's.[36] However, the decay behavior becomes exponential above 22 K, and the lifetime reduces dramatically to 23 ns at 24 K due to the increased thermally activated hopping.[36] Furthermore, stretched exponentials on the order of a few μs have not previously been reported for AlAs/GaAs d-SL's. This comparison suggests that the intentionally maintained 4-ML period may influence the band structure of the d-SL in a way that enhances the depth and density of localized states in the band tail. In comparison to the PL intensity from the RBA or o-(2,2) SL, the PL emission at long time from both d-SL's is orders of magnitude more intense, further supporting the description that the long-lived recombination process is associated with localized carriers in a random potential and not a long-lived indirect process.

IV. DISCUSSION

A number of previously reported observations[8-13] of general properties of disordered superlattices have been repeated. Although not normally noteworthy, this confirmation is significant because of the variations inherent in any random system and also due to the different constraints on the disordering scheme employed. These properties were also confirmed using other techniques. Specifically, both PLE and PR show a redshift in the band gap as well as the generation of a high density of states at energies below the band gap in the d-(1,3) SL compared to either the RBA or the o-(2,2) SL having the same overall compositions. Both the redshift and the large number of band-tail states are also commonly seen in ordered alloys,[37] where they are believed to result from a broad distribution of band gaps.[5] The observed redshift and band-tail states are independent of whether the constraint on the disordering scheme is (a) m, n in $(GaAs)_m(AlAs)_n$ d-SL's with equal probabilities;[9] (b) the probability of the 2 ML layers is twice that of 1- and 3-ML layers;[9] or (c) $n,4-n$ in $(GaAs)_n(AlAs)_{4-n}$ d-SL's (this work) where $n=[0,1,2,3,4]$ or $[1,2,3]$. Equivalence of the optical properties also suggests that the heterointerfaces obtained under the growth conditions we have employed are similar to those obtained with 3-5-s growth interrupts used during deposition at a higher temperature and at twice the growth rate. Time-resolved PL

measurements at 50 K, which show a stretched exponential decay of the luminescence, give definitive confirmation that disorder-induced carrier localization is dominating the optical properties of *d*-SL's.

In the *d*-(0,4) SL, the constraints on layer thickness were chosen to allow the possibility of zero ML of either component, leading to wells and barriers as thick as 11 and 14 ML, respectively. The appearance of these wider regions led to a structure with properties intermediate between the those of the *d*-(1,3) SL with narrower constraints and true multiple single quantum wells (MSQW's). Specifically, intense low-energy emission from the *d*-(0,4) SL is more pronounced than that from the *d*-(1,3) SL. However, the PL has only very weak spectral dependence on either temperature or excitation intensity, characteristic of MSQW's and very different from the dependences of the *d*-(1,3) SL. Furthermore, the TRPL of the *d*-(0,4) SL shows a temperature-dependent short lifetime component characteristic of QW structures and the existence of a long-lived component characteristic of localized carriers.

Insights into the properties of *d*-SL's were gained by use of MMPL, which indicates that carriers ionized by the microwaves are able to migrate to nearby (spatially) potential minima lower in energy than those which dominate the PL. In the case of the *d*-(1,3) SL, this behavior is consistent with the more rapid disappearance of the higher-energy PL emissions with increasing temperature. Both observations indicate the dominant PL processes involve metastable states. Similar MMPL spectra are also seen for ordered III-V alloys,[31] which exhibit a similar broad spectral and spatial distribution of band gaps. In both disordered superlattices and natural, inhomogeneously ordered alloys, the dominant PL processes involve metastable states, high densities of states below an ill-defined band gap and thermally coupled MMPL spectra in which carriers ionized from the dominant processes reappear at lower energy. Several optical characteristics of the ordered alloys, most notably emission energies and lifetimes which are strong functions of excitation intensity, are not observed in these *d*-SL's. Hence we report some similarities but also some differences among the optical properties of inhomogeneously ordered alloys and one-dimensional disordered superlattices. Moreover, we can generally state that the physics of inhomogeneously spontaneously ordered alloys is governed by zone folding and level repulsion, and is well characterized by long-range order.[1] In contrast, the physics of *d*-SL systems, including those with long-range order that we have defined as $(GaAs)_n(AlAs)_{4-n}$, is governed by short-range disorder and is well described by carrier localization.

V. CONCLUSIONS

We have reported the optical properties of different atomic arrangements of $Al_{0.5}Ga_{0.5}As$, deposited by molecular-beam epitaxy and having nominally identical average composition. We observe unique optical signatures for a random pseudobinary alloy and $(AlAs)_n(GaAs)_{4-n}$ superlattices where $n=2$ (ordered) or n is randomly chosen (disordered) from the sets [1,2,3] or [0,1,2,3,4]. When $n=$[0, 1, 2, 3, or 4] the optical properties are dominated by quantum confinement effects due to the presence of layers with thicknesses up to 14 monolayers. When $n=$[1, 2, or 3] the optical properties are consistently described by the presence of disorder-induced localized states and a hopping-assisted recombination mechanism. We have also reported observation of stretched exponentials in low-temperature TRPL from a monolayer AlAs/GaAs *d*-SL. This observation confirms that disorder-induced carrier localization is dominating the observed properties. Further investigations and theoretical considerations will elucidate the importance of the layer purity, thicknesses, and overall degree of disorder on the electro-optical properties and potential applicability of our materials.

ACKNOWLEDGMENTS

Helpful discussions with H. Branz, A. Zunger, K. Mäder, and S.-H. Wei, and the support of W. Moore and W. Westwood, are gratefully acknowledged. Part of this work was supported by the U.S. Department of Energy, Office of Energy Research, Division of Basic Energy Sciences and by Contract No. DE-AC02-83CH10093 and NREL Contract No.XR-2-12121-1. M.C.D., D.J.M., and M.S.S. wish to acknowledge the support of a NATO Collaborative Research Grant.

[1] A. Zunger and S. Mahajan, *Atomic Ordering and Phase Separation in Epitaxial III-V Alloys,* Handbook on Semiconductors Vol. 3, 2nd ed. (Elsevier, Amsterdam, 1994).

[2] A. Gomyo, K. Kobayashi, S. Kawata, I. Hino, T. Suzuki, and T. Yuasa, J. Cryst. Growth. **77**, 367 (1986).

[3] D. J. Friedman, A. E. Kibbler, and J. M. Olson, Appl. Phys. Lett. **59**, 2928 (1991).

[4] D. B. Laks, S.-H. Wei, and A. Zunger, Phys. Rev. B **69**, 3766 (1992).

[5] G. S. Horner, A. Mascarenhas, S. Froyen, R. G. Alonso, K. A. Bertness, and J. M. Olson, Phys. Rev. B **47**, 4041 (1993).

[6] A. Chomette, B. Deveaud, A. Regreny, and G. Bastard, Phys. Rev. Lett. **57**, 1464 (1986).

[7] E. Tuncel and L. Pavesi, Philos. Mag. B **65**, 213 (1992), and references therein.

[8] A. Sasaki, M. Kasu, T. Yamamoto, and S. Noda, Jpn. J. Appl. Phys. **28**, L1249 (1989).

[9] M. Kasu, T. Yamamoto, S. Noda, and A. Sasaki, Jpn. J. Appl. Phys. **29**, 828 (1990).

[10] M. Kasu, T. Yamamoto, S. Noda, and A. Sasaki, Jpn. J. Appl. Phys. **29**, L1055 (1990).

[11] M. Kasu, T. Yamamoto, S. Noda, and A. Sasaki, Appl. Phys. Lett. **59**, 800 (1991).

[12] M. Kasu, T. Yamamoto, S. Noda, and A. Sasaki, Jpn. J. Appl.

Phys. **29**, L1588 (1990).
[13]A. Sasaki, J. Cryst. Growth **115**, 490 (1991).
[14]X.-L. Wang, A. Wakahara, and A. Sasaki, Appl. Phys. Lett. **62**, 888 (1993).
[15]X. Chen, B. Henderson, and K. P. O'Donnell, Appl. Phys. Lett. **60**, 2672 (1992).
[16]K. F. Brennan, Appl. Phys. Lett. **57**, 1114 (1990).
[17]W. P. Su and H. D. Shih, J. Appl. Phys. **72**, 2080 (1992).
[18]J. Strozier, Y. A. Zhang, C. Hortorn, A. Ingatiev, and H. D. Shih, J. Vac. Sci. Technol. A **11**, 923 (1993).
[19]P. W. Anderson, Phys. Rev. **109**, 1492 (1958).
[20]A. J. SpringThorpe, T. P. Humphreys, A. Majeed, and W. T. Moore, Appl. Phys. Lett. **55**, 2138 (1989).
[21]L. E. Tarof, C. J. Miner, and A. J. SpringThorpe, J. Electron. Mater. **18**, 361 (1989).
[22]J. Grant, J. Menéndez, L. N. Peiffer, K. W. West, E. Molinari, and S. Baroni, Appl. Phys. Lett. **59**, 2859 (1991).
[23]M. C. DeLong, I. Viohl, W. D. Ohlsen, P. C. Taylor, F. P. Dabkowski, K. Meehan, J. E. Williams and M. Hopkinson, in *Spectroscopic Characterization Techniques for Semiconductor Technology IV,* edited by Orest J. Glembocki (SPIE, Bellingham, WA, 1992), Vol. 1678, p. 221.
[24]R. K. Ahrenkiel, D. J. Dunlavy, and T. Hanak, Solar Cells **24**, 339 (1988).
[25]M. Cardonna, *Modulation Spectroscopy* (Academic, New York, 1969); D. E. Aspnes, in *Handbook on Semiconductors,* edited by T. S. Moss (North-Holland, New York, 1980), Vol. 2, p. 109.
[26]W. Ge, M. D. Sturge, W. D. Schmidt, L. N. Pfeiffer, and K. W. West, Appl. Phys. Lett. **57**, 55 (1990).
[27]S.-H. Wei and A. Zunger, J. Appl. Phys. **63**, 5794 (1988).
[28]N. Mott, and E. A. Davis, *Electronic Processes in Non-Crystalline Materials* (Clarendon, Oxford, 1979).
[29]T. Yamamoto, M. Kasu, S. Noda, and A. Sasaki, J. Appl. Phys. **68**, 5318 (1990).
[30]C. G. Van de Walle and R. M. Martin, Phys. Rev. B **35**, 8154 (1987).
[31]M. C. DeLong, W. D. Ohlsen, I. Viohl, X. Yin, P. C. Taylor, D. Sengupta, G. E. Stillman, J. M. Olson, and W. A. Harrison, Phys. Rev. B **43**, 1510 (1993).
[32]M. Gurioli, J. Martinez-Pastor, M. Colocci, C. Deparis, B. Chastaingt, and J. Massies, Phys. Rev. B **46**, 6922 (1992).
[33]H. Takayasu, *Fractals in the Physical Sciences* (MUP, Manchester, UK, 1990).
[34]R. S. Crandall, Phys. Rev. B **43**, 4057 (1991).
[35]A. K. Jonscher, in *Nonexponential Relaxations in Disordered Systems (Structure and Bonding in Noncrystalline Solids),* edited by G. E. Walrafen and A. G. Revesz (Plenum, New York, 1986), pp. 101–107.
[36]G. D. Gilliland, D. J. Wolford, J. A. Bradley, J. Klem, and M. Jaros, J. Vac. Sci. Technol. B **11**, 1647 (1993).
[37]M. C. DeLong, D. J. Mowbray, R. A. Hogg, M. S. Skolnick, M. Hopkinson, J. P. R. David, P. C. Taylor, Sarah R. Kurtz, and J. M. Olson, J. Appl. Phys. **73**, 5163 (1993).

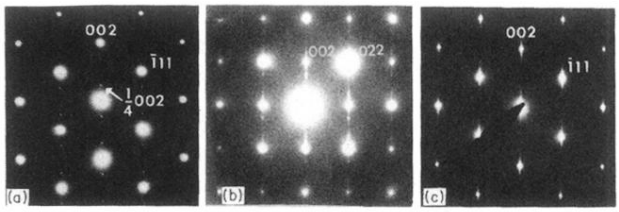

FIG. 1. Transmission electron diffraction image of (a) *o*-(2,2) SL, (b) *d*-(1,3) SL, and (c) *d*-(0,4) SL. The extra spots near the $\frac{1}{2}(001)$ positions confirm the long-range order of the SL samples. The additional spotty streaks in (b) and (c) are associated with the random sequencing employed, which effectively produces sections of the SL with longer periodicity. Note that Figs. (a) and (c) were taken with the electron beam parallel to a [110] zone axis, while Fig. (b) was recorded with the electron beam parallel to a [100] zone axis.

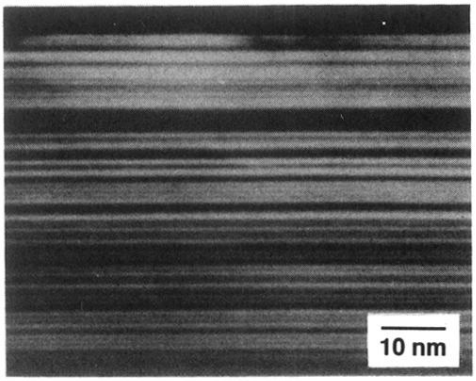

FIG. 2. A (004) dark-field transmission electron micrograph of the *d*-(0,4) SL displaying periodic variations associated with the random sequencing of the GaAs and AlAs layers. The relatively wide dark band located in the upper portion of the image is produced with the sequence $(AlAs)_2(GaAs)_2$ followed by two $(GaAs)_4(AlAs)_0$ subunits, effectively producing a $(GaAs)_{10}$ layer.